The SMBHB candidate 3C 66A

Bologna, 2025.10.28

Towards high-performance mm-VLBI science operations with multi-band receivers workshop

By Paloma Thevenet[1,2]
In collaboration with: Bong Won Sohn[1], Guang-Yao Zhao[3,1], Jeong-Uk Kim[4,1], Suk-Jin Yoon[4]

[1]: KASI, [2]: Observatoire de Paris, [3]: MPIfRA, [4]: Yonsei University

Summary

1) Introduction
2) Observations of 3C 66A
   - KaVA data
   - VLBA data
   - Multiwavelength data
3) Analysis of the oscillating jet
   - Jet precession model
   - A supermassive black hole binary (SMBHB) candidate
   - Possible Lense-Thirring effect
   - Other disk or jet instabilities
4) Conclusions

1. Introduction: blazars

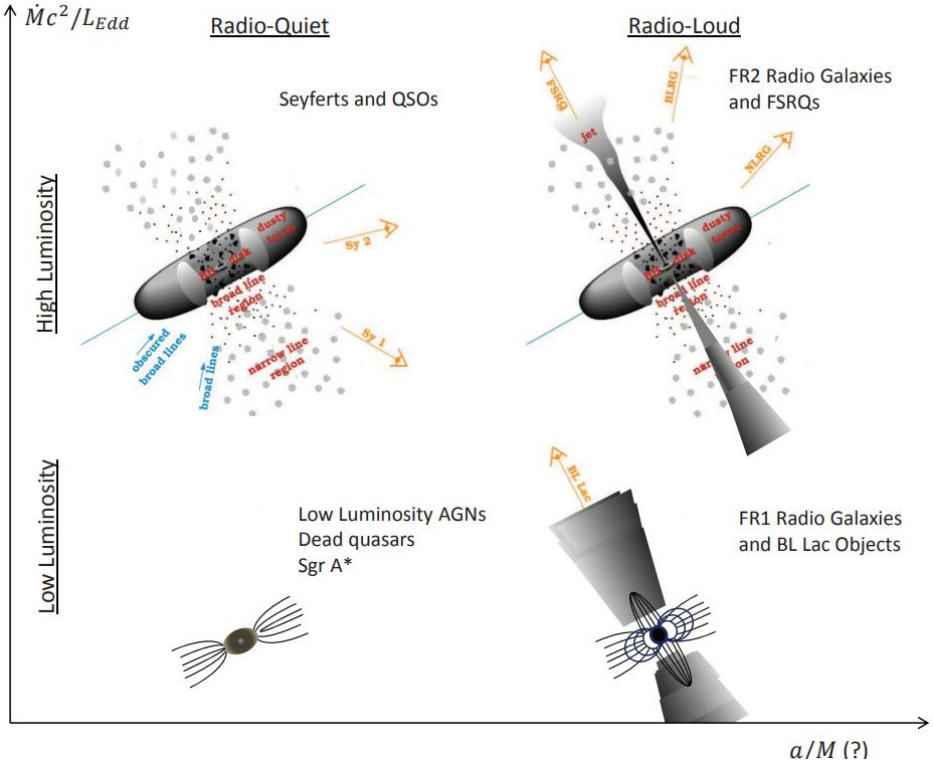

~10% of AGNs are radio loud (RL) and launch a relativistic jet through the Blandford-Znajek (BZ) or Blandford-Payne (BP) mechanism.

We call blazars RL AGNs with jets closely aligned to the line of sight.

Illustration of an AGN unification model (Dermer&Giebels+16)

2) Observations of 3C 66A

2. KaVA data

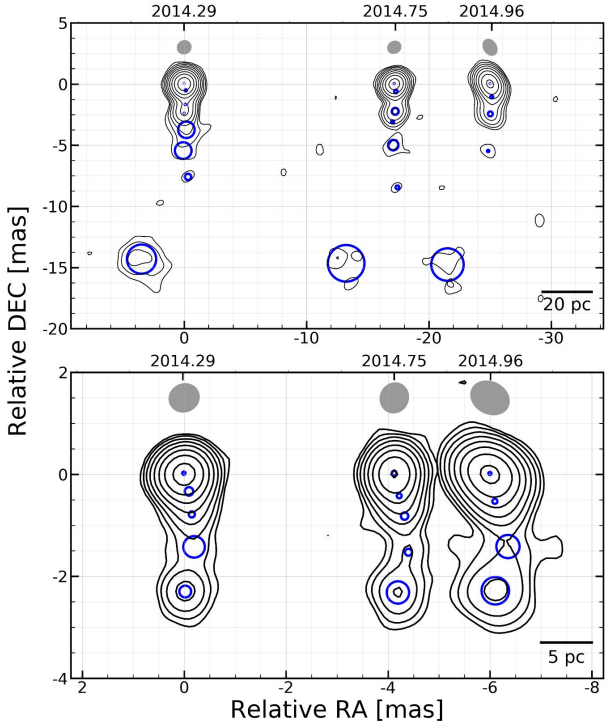

3C 66A is a BL Lac object at z~0.340 (1 mas ~ 5 pc), presenting numerous jet bendings and complex kinematics (apparent superluminal components, transverse motions…).

We find a twisted pc-scale jet structure in the KaVa (KVN and VERA array) map at 22 GHz.

KaVA intensity maps of the 3C 66A radio jet at 22 GHz (top) and 43 GHz (bottom) in 2014

2. VLBA data

We analyse the position angle (PA) evolution of three jet regions over 29 years of 43 GHz VLBA data using two methods: circular Gaussian fitting (DIFMAP) and annular binning.

The PA in the 2 regions close to the core oscillates and decays, while the furthest region's PA only undergoes decay.

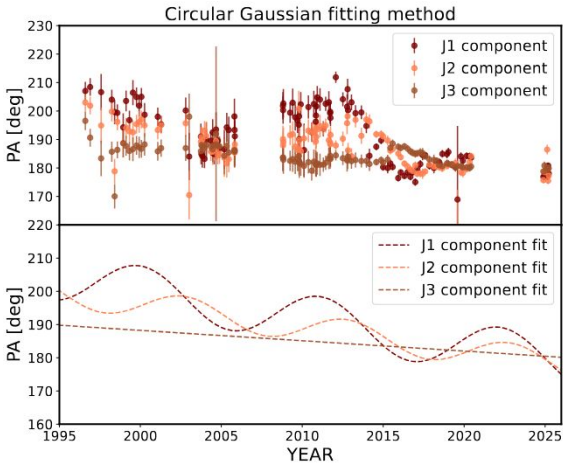

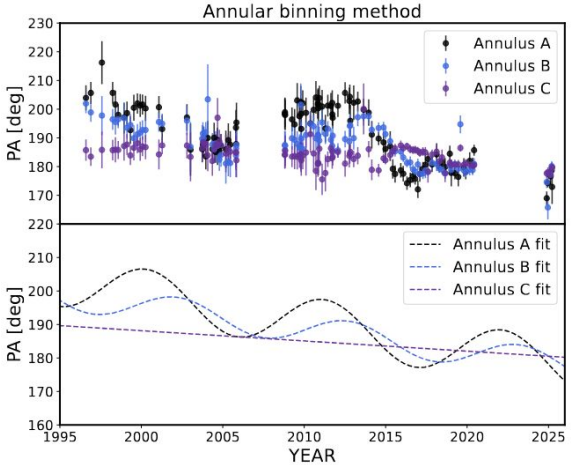

2. VLBA data

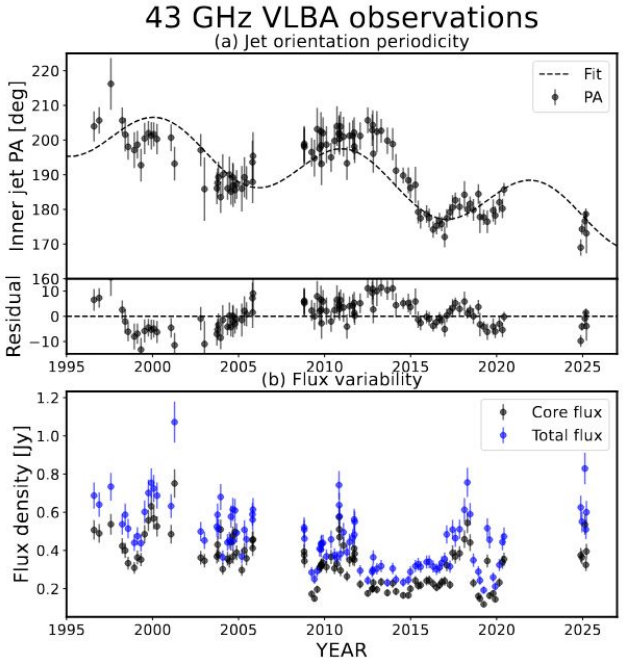

(a) Inner jet PA versus time at 43 GHz. (b) Time evolution of the total (blue) and core (black) flux density

The inner jet PA oscillates every ~11 years (5σ detection) with amplitude ~8° and re-orients at a rate of -0.8°/yr.

The dominant core flux density is highly variable with a baseline decrease and possible quasi-periodicities (2σ detection) of ~3, ~7, ~10 years.

Discrete correlation function analysis reveals a possible (2σ detection) correlation between the inner jet PA and the core flux density.

2. Multiwavelength data

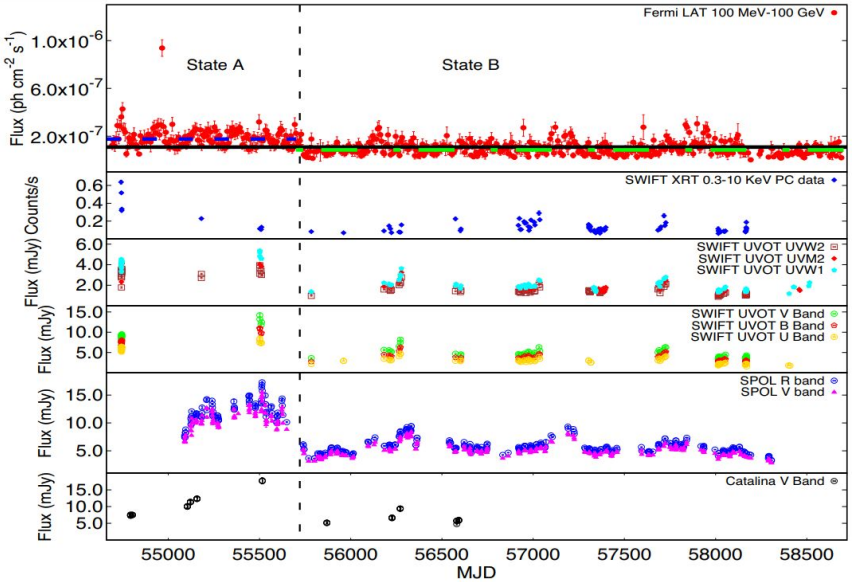

Multiwavelength LCs of 3C 66A showing a baseline drop (Mohana+21)

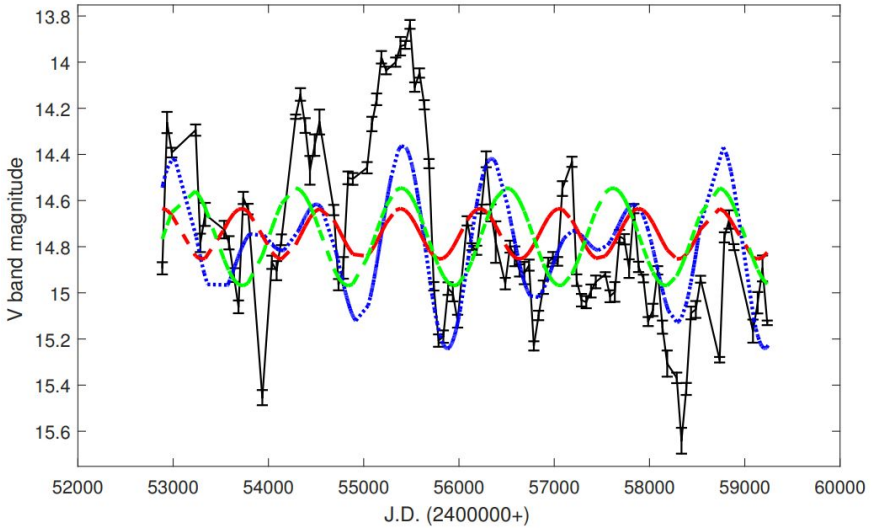

Optical LC of 3C 66A and detected sinusoidal periodicities (Cheng+22)

3) Analysis of the oscillating jet

3. Jet precession model

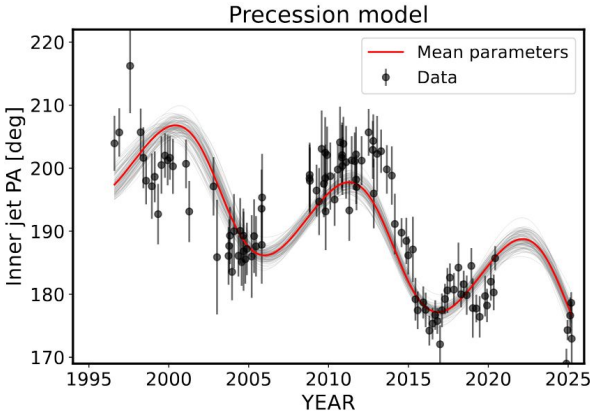

Precession fit to the inner jet PA for 100 random MCMC samples and mean parameters.

Half-opening angle of the cone,	Ω	0.47 ± 0.17	°
Precession period,	P_p	10.88 ± 0.24	yr
Reference time,	t_0	2016.80 ± 0.14	yr
Angle between the precession cone axis and the line fo sight,	ϕ_0	3.32 ± 1.18	°
Projected angle of the cone axis onto the sky plane,	θ_0	185.19 ± 0.51	°

The PA oscillation and slow re-orientation possibly correlated to the core flux density, and the ~2 years optical flux periodicity indicate a geometric scenario.

We interpret the PA data as a precessing jet over 2 timescales: decadal and secular. We fit the ~11 year period with a precessing nozzle model.

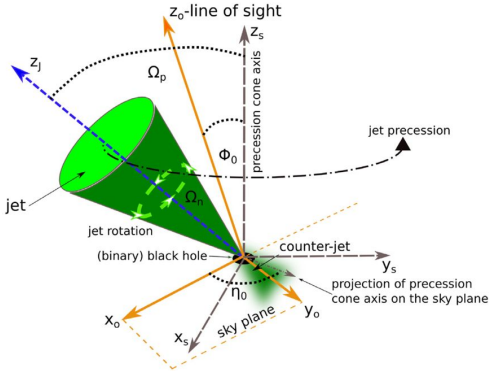

Geometry of a precessing jet (Britzen+18)

3. A SMBHB candidate

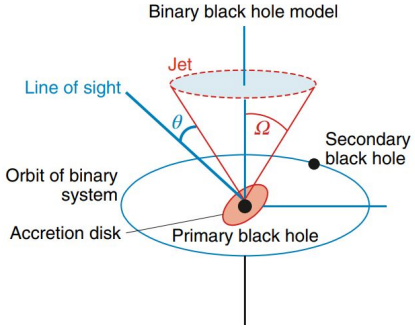

Potential geometry of a SMBHB system inducing disk-orbit jet precession (Abraham+18)

SMBHBs can lead to periodic orientation changes through several mechanisms: orbital motion, BH spin/orbital plane misalignment, accretion disk/orbital plane misalignment etc...

Flux periodicity can be further induced by mechanisms related to perturbation of the disk(s).

Ex: Interpretation of jet oscillation in S5 1928+738 (Kun+14,+23), OJ287 (Britzen+18, +23), M81 (Jiang+23) and many others.

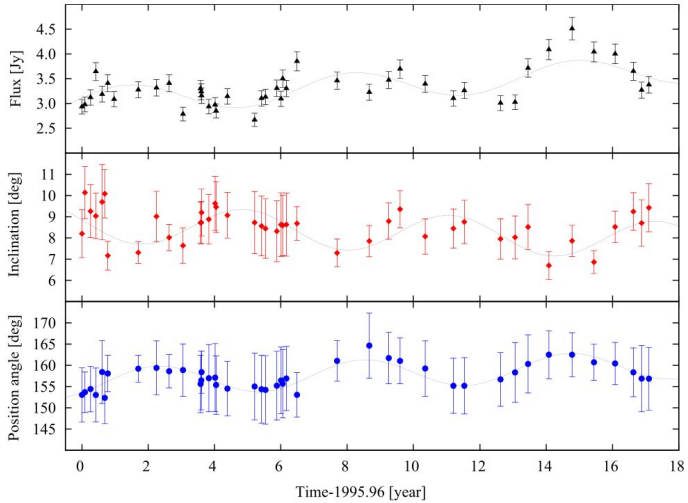

Total flux density of the jet at 15 GHz (top), inclination (middle) and PA (bottom) of the jet geometrical axis plotted against time (Kun+14)

3. A SMBHB candidate

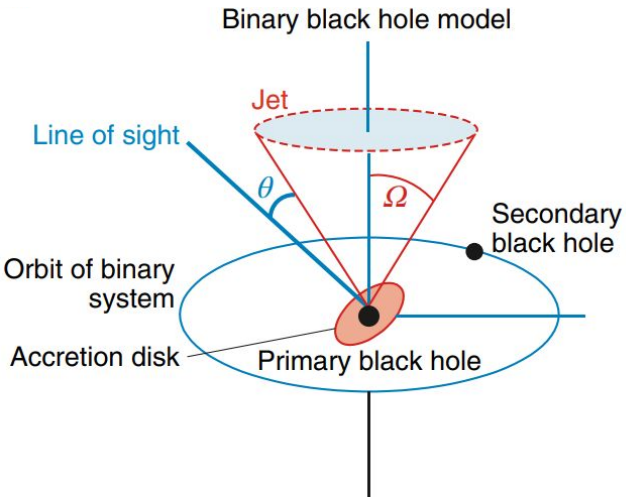

Potential geometry of a SMBHB system inducing disk-orbit jet precession (Abraham+18)

The short- and long-term precession timescales of 3C 66A can, respectively, be associated with orbital motion and disk/orbit precession in a SMBHB system.

We estimate the system parameters:

Total mass,	M	1.42 ± 0.19	$10^8\ M_\odot$
Mass ratio,	q	0.18 ± 0.15	
Observed period,	$P_{\rm obs}$	10.88 ± 0.24	yr
Orbital period,	$P^{\rm orb}$	16.72 ± 0.42	yr
Separation,	$r_{\rm sep}$	1.65 ± 0.08	10^{-2} pc
PN parameter,	ϵ	4.10 ± 0.58	10^{-4}
Merger timescale,	$T_{\rm merge}$	≈ 934	Myr
Strain amplitude,	h	≈ 3.93	10^{-19}

3. A SMBHB candidate

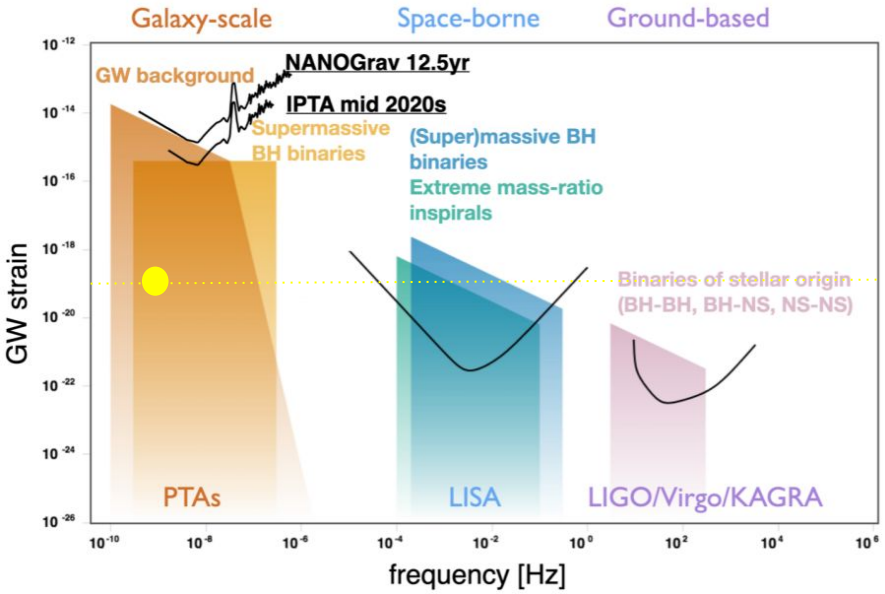

Overview of the GW spectrum, detectors and source populations as a function of GW frequency, adapted from Moore+15

The short- and long-term precession timescales of 3C 66A can, respectively, be associated with orbital motion and disk/orbit precession in a SMBHB system.

We estimate the system parameters:

Total mass,	M	1.42 ± 0.19	$10^8\ M_\odot$
Mass ratio,	q	0.18 ± 0.15	
Observed period,	$P_{\rm obs}$	10.88 ± 0.24	yr
Orbital period,	$P^{\rm orb}$	16.72 ± 0.42	yr
Separation,	$r_{\rm sep}$	1.65 ± 0.08	10^{-2} pc
PN parameter,	ϵ	4.10 ± 0.58	10^{-4}
Merger timescale,	$T_{\rm merge}$	≈ 934	Myr
Strain amplitude,	h	≈ 3.93	10^{-19}

3. Possible Lense-Thirring effect

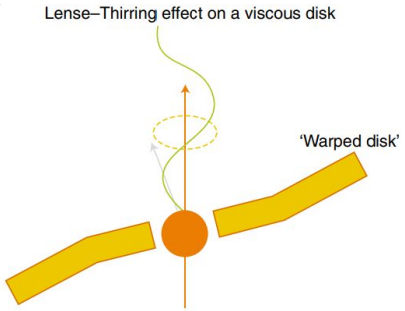

Schematic geometry of an accretion disk and BH angular momentum misalignment (Abraham+18)

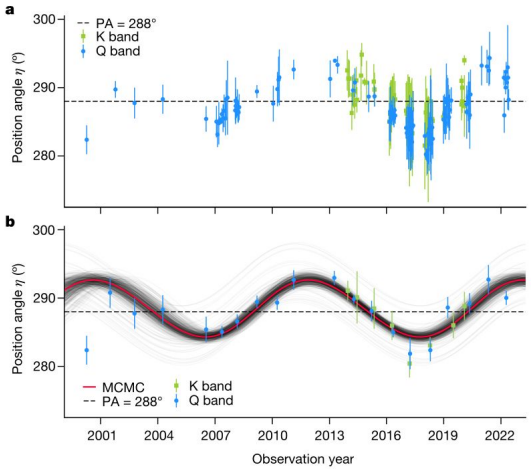

a) Evolution of the position angle (PA) of the M87 jet and b) fit of the yearly binned PA with a precession model (Cui+23)

LT precession corresponds to the precession of a viscous accretion disk misaligned with the BH spin due to frame-dragging effects (Bardeen-Petterson).

Precession can be extended to the entire disk-jet system, supported by GRMHD simulations (Liska+18), as expected through the BP or BZ mechanisms.

Ex: Interpretation for the oscillating jet in 3C 454.3 (Qian+14) or M87 (Cui+23).

3. Possible Lense-Thirring effect

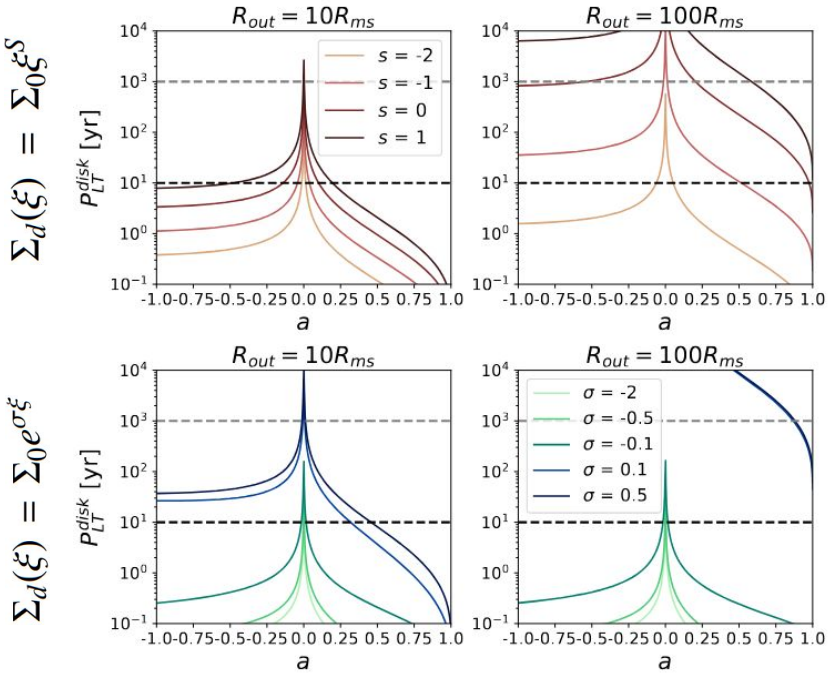

Lense-Thirring disk precession can explain either the short- or long-term PA evolution timescales for 3C 66A.

A power-law disk density profile allows a wider range of spin parameters in either case.

Period of LT disk precession as a function of the spin parameter, outer radius and density power law slope s (upper panel) or density exponential factor σ (lower panel).

3. Other disk or jet instabilities

- Disk-induced precession (Lu 1992) cannot account for any observed periodicity in 3C 66A of the primary would have a basically null spin.

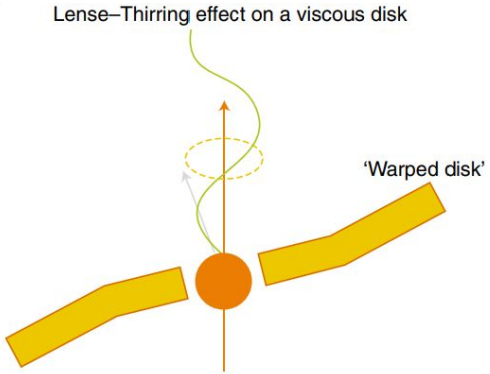

Schematic geometry of an accretion disk and BH angular momentum misalignment (Abraham+18)

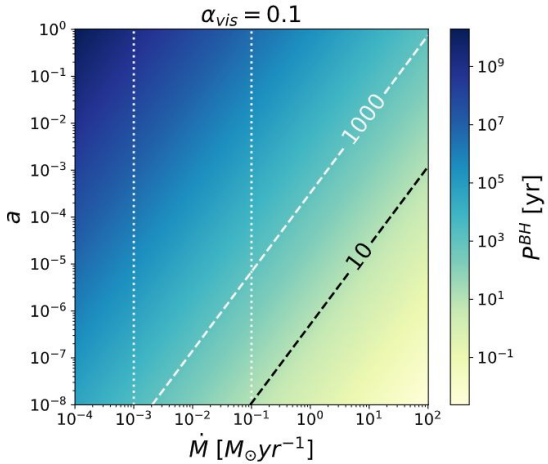

2D plot of the precession period as a function of the spin parameter and the accretion rate. The opaque area highlights the typical range of accretion rates for BL Lac objects.

3. Other disk or jet instabilities

- CD kink instability: the CDI growing timescale fits the expected jet properties, and can explain the ~11 years periodic PA pattern.

The kink instability develops in the presence of strong toroidal magnetic fields, leading to helical jet distortion.

Ex: Interpretation for a ~13 hours quasi-periodic flux oscillation in BL Lacertae (Jorstad+22).

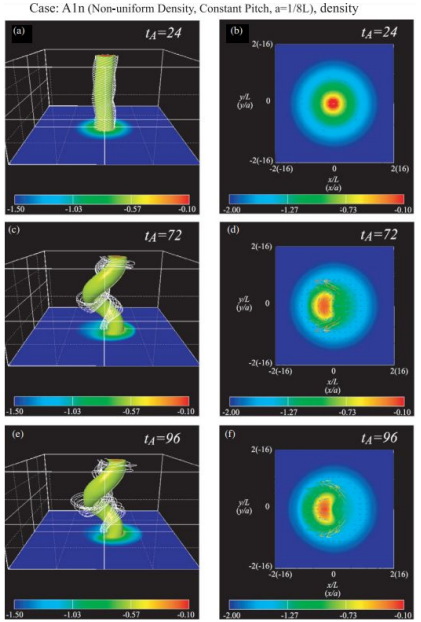

Development of the kink instability through 3D RMHD simulations (Mizuno+09)

3. Other disk or jet instabilities

- KH helical instability: possible interpretation for the ~11 years periodic PA pattern, assuming that it corresponds to a propagating wave, for an Alfvènic jet with an external medium of comparable magnetization to the jet.

The KHI arises at the interface between the jet and the external medium where there is a velocity gradient. The helical mode has been used to explain twisted structures and swinging jets.

Ex: Interpretation of the twisted jets of 3C 449 (Hardee+81) and of a ~10 year quasi-periodic orientation pattern in M87 (Walker+18), as well as its jet base morphology (Matveyenko&Seleznev+15).

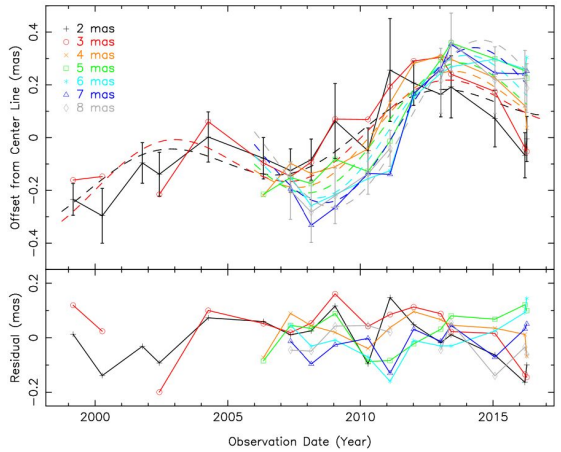

Measured offsets of the M87 jet center from a line extending from the core along position angle of −72° (Walker+18)

3. Other disk or jet instabilities

- Radiation-induced disk warping: the characteristic timescale is several orders of magnitude larger than both the short- and long-term periods observed.

An optically thick accretion disk irradiated by a central source is unstable to becoming non-planar or warped (Pringle+96, +97).

Ex: Possible explanation for jet precession at the center of the galaxy NGC 1275 (Dunn+09).

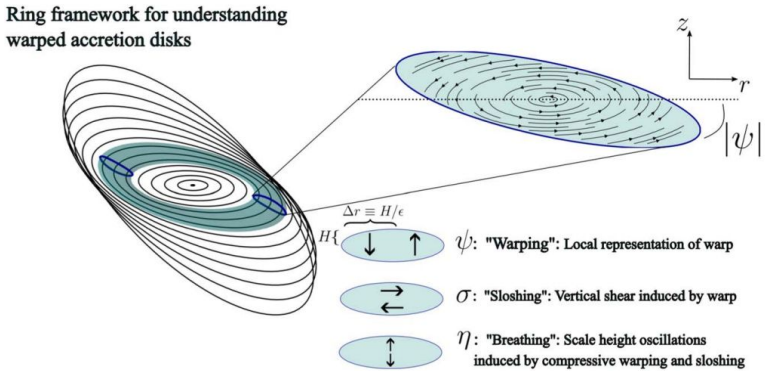

Warped disk depicted with a series of concentric annuli (black) with radially dependent orientations (Kaaz+25)

3. Other disk or jet instabilities

- Disk-induced BH spin-axis precession cannot account for any observed periodicity in 3C 66A of the primary would have a basically null spin.

- **CD kink instability:** the CDI growing timescale fits the expected jet properties, and can explain the ~11 years periodic PA pattern.

- **KH helical instability**: possible interpretation for the ~11 years periodic PA pattern, assuming that it corresponds to a propagating wave, for an Alfvènic jet with an external medium of comparable magnetization to the jet.

- Radiation-induced disk warping: the characteristic timescale is several orders of magnitude larger than both the short- and long-term periods observed.

4. Conclusions

3C 66A has a twisted jet showing periodic PA changes on 2 timescales, known flux periodicity and possible radio periodicity, interpreted as:

1) a precessing jet in a SMBHB system, or

2) a precessing jet due to Lense-Thirring of the disk combined with CDI or KHI propagation.

Thank you

Extra slides

3C 66A: PA and CFD correlation

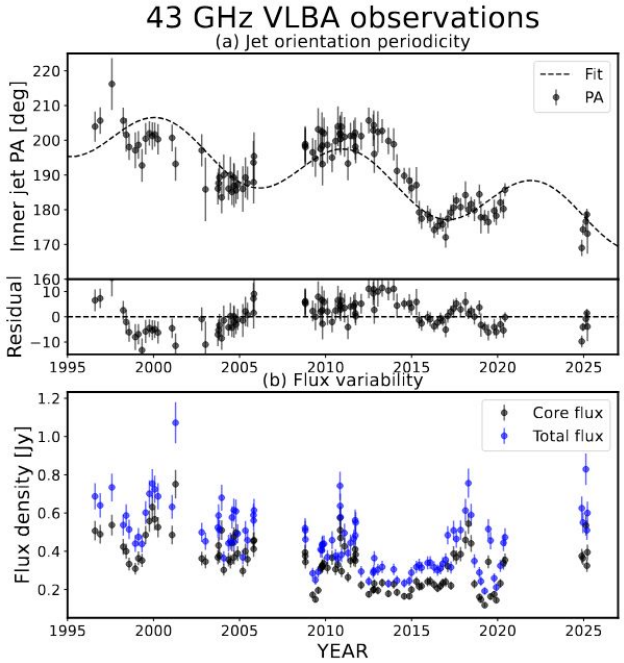

(a) Inner jet PA versus time at 43 GHz. (b) Time evolution of the total (blue) and core (black) flux density

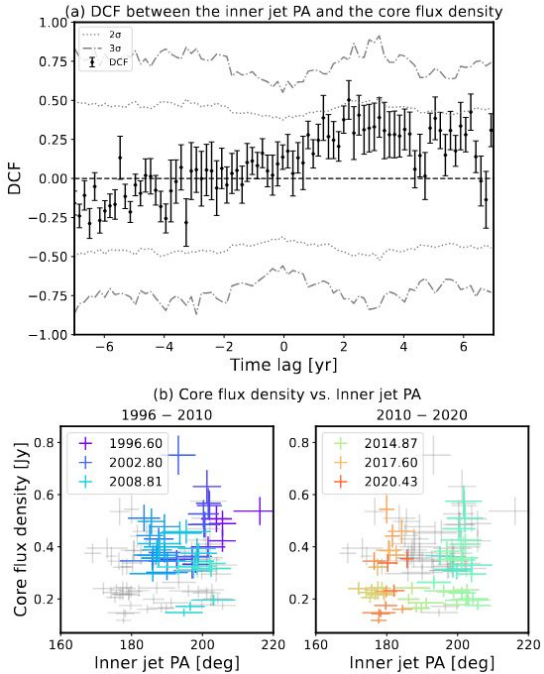

a) Discrete correlation function (DCF) analysis between the PA and the core flux density; and b) inner jet PA vs core flux density on each PA period rise/decay phase.

3C 66A: PA periodicity analysis

1 - Jurkevic analysis

$$F = \frac{1 - V_m^2}{V_m^2}$$

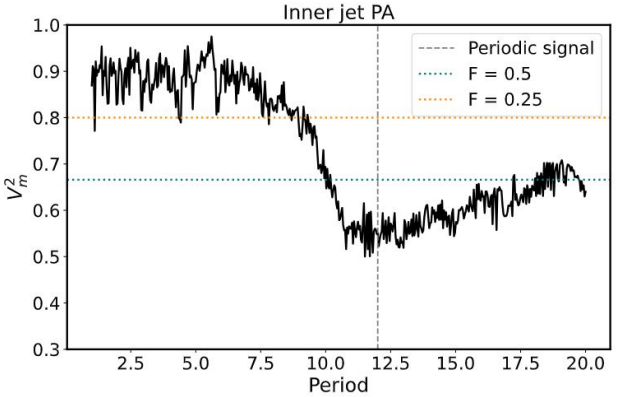

2 - Lomb-Scargle periodogram

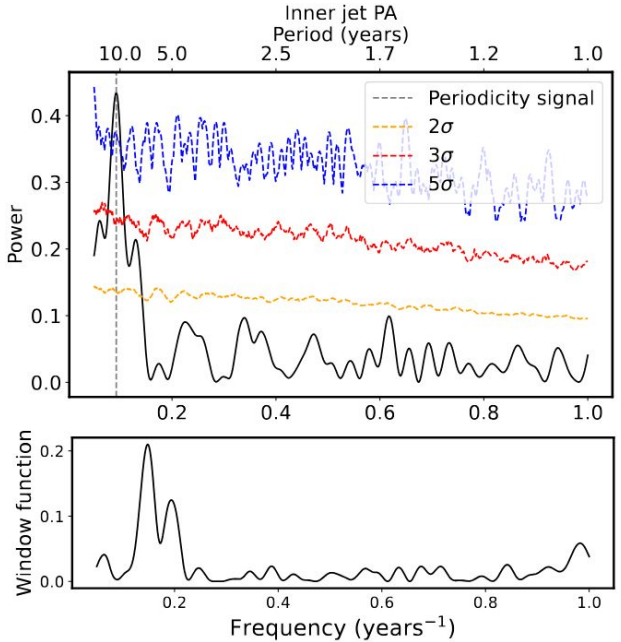

3 - Weighted wavelet z-transform

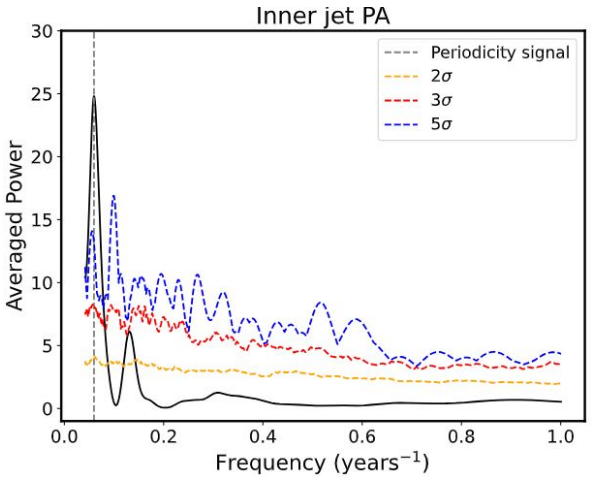

3C 66A: CFD periodicity analysis

1 - Jurkevic analysis

$$F = \frac{1 - V_m^2}{V_m^2}$$

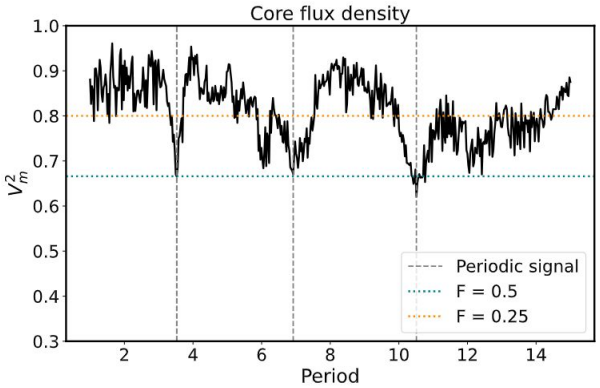

2 - Lomb-Scargle periodogram

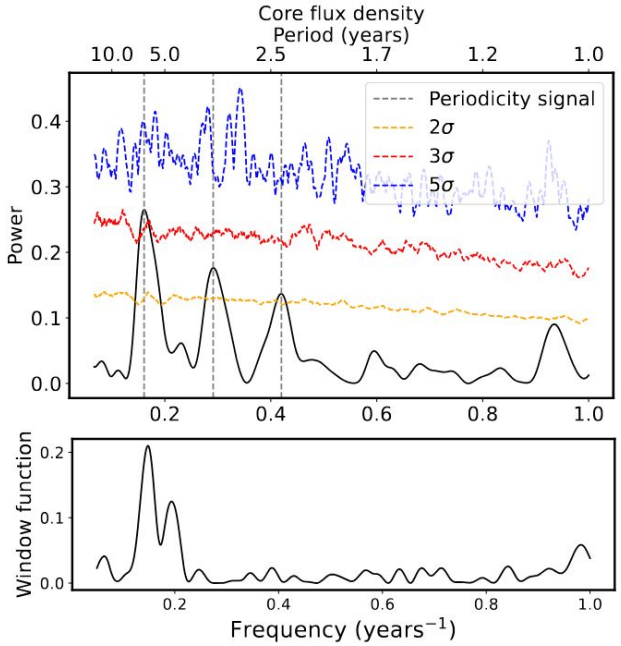

3 - Weighted wavelet z-transform

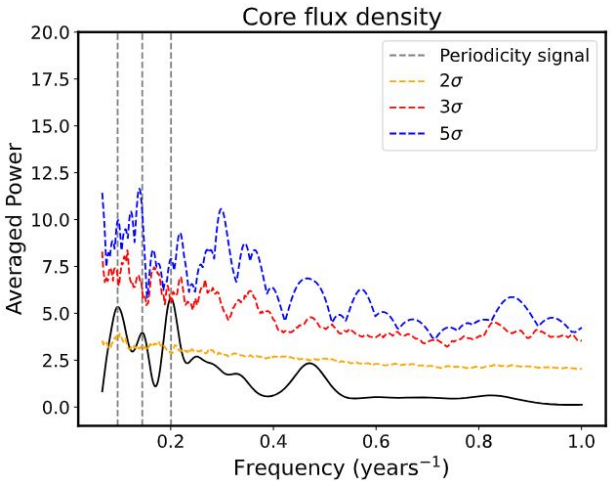

3C 66A: jet precession model

$$\eta(t) = \arctan\left(\frac{y(t)}{x(t)}\right),$$

with Cartesian coordinates in the observer's frame,

$$x(t) = A(t)\cos\eta_0 - B(t)\sin\eta_0,$$
$$y(t) = A(t)\sin\eta_0 + B(t)\cos\eta_0,$$

and with

$$A(t) = \cos\Omega\sin\Phi_0 + \sin\Omega\cos\phi_0\sin\omega(t - t_0),$$

$$B(t) = \sin\Omega\cos\omega(t - t_0),$$

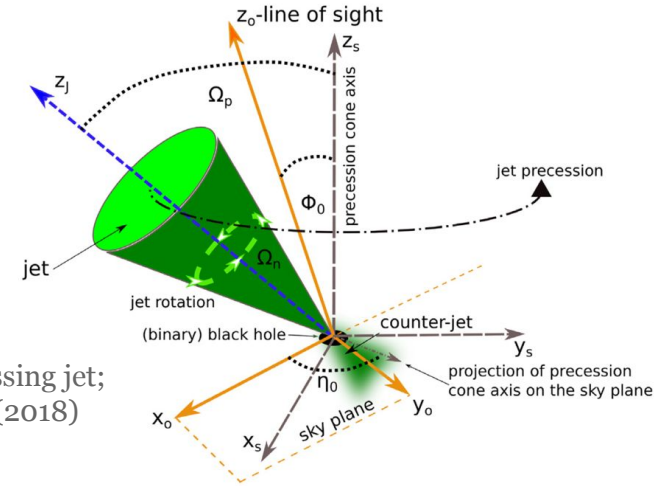

Geometry of a precessing jet; credit: Britzen et al. (2018)

Half-opening angle of the cone,	Ω	0.47 ± 0.17	°
Precession period,	P_p	10.88 ± 0.24	yr
Reference time,	t_0	2016.80 ± 0.14	yr
Angle between the precession cone axis and the line fo sight,	ϕ_0	3.32 ± 1.18	°
Projected angle of the cone axis onto the sky plane,	θ_0	185.19 ± 0.51	°

3C 66A: jet precession model

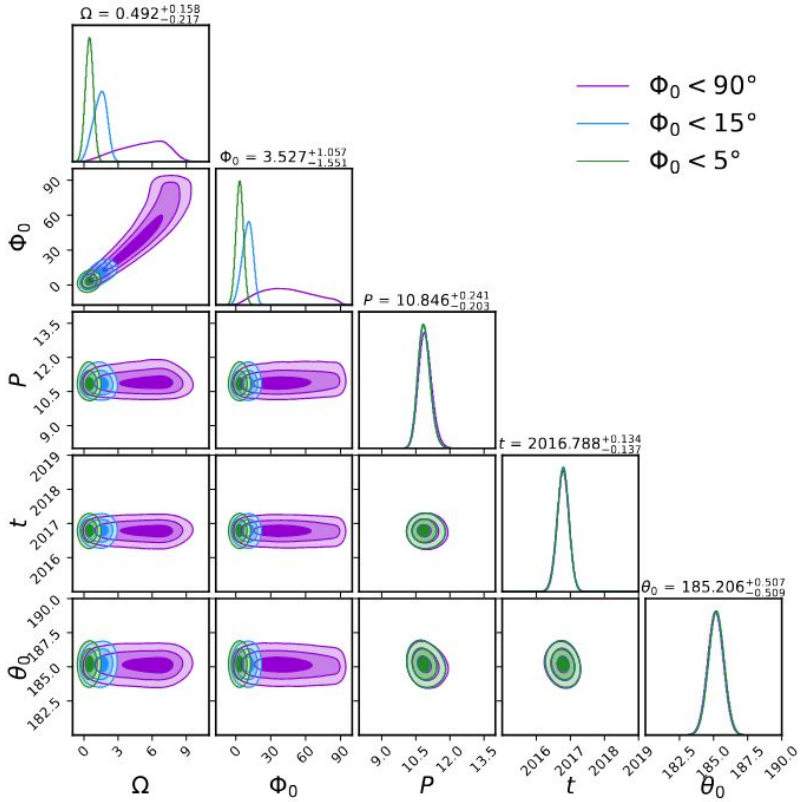

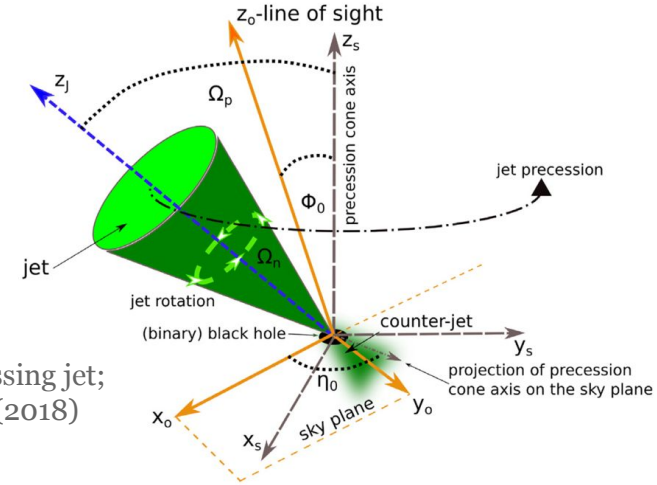

Geometry of a precessing jet; credit: Britzen et al. (2018)

Half-opening angle of the cone,	Ω	0.47 ± 0.17	°
Precession period,	P_p	10.88 ± 0.24	yr
Reference time,	t_0	2016.80 ± 0.14	yr
Angle between the precession cone axis and the line fo sight,	ϕ_0	3.32 ± 1.18	°
Projected angle of the cone axis onto the sky plane,	θ_0	185.19 ± 0.51	°

3C 66A: precession-driven Alfvèn waves

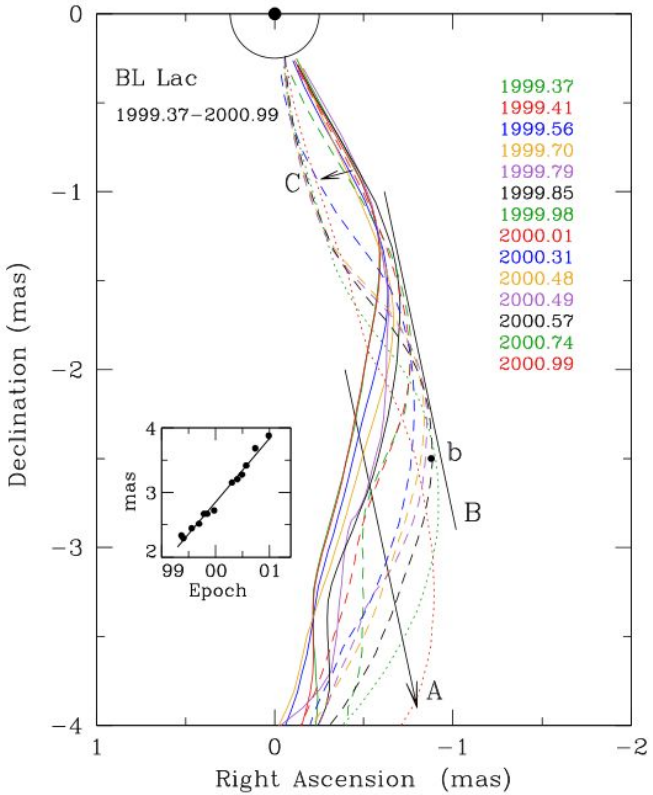

Comparison with the jet displacement observed in BL Lac (Cohen et al. 2015):

- Transverse patterns that propagate superluminally downstream
- Interpreted as Alfvén waves propagating on the longitudinal component of a helical magnetic field
- The waves may be excited by the swinging of a recollimation shock component
- Compared to 3C 66A: presumed wave of equivalent apparent speed of about 5c, propagating over similar spatial scales (order of 10 pc deprojected), which may be excited by nozzle precession
- Difference: the patterns are highly variable, with periods of about 1 year

Ridge lines for BL Lac at 15 GHz for 14 epochs between 1999.37 and 2000.99; Cohen et al. (2015

What are ‘swinging’ jets?

In the literature, we encounter jets described with the terms: *curved, bent, twisted, kink, twisting, wobble, wobbling, wiggle, wiggling, swinging, oscillating…*

Curved or *bent/twisted*: a jet that presents a curvature/several curvatures in different directions (at a given time)

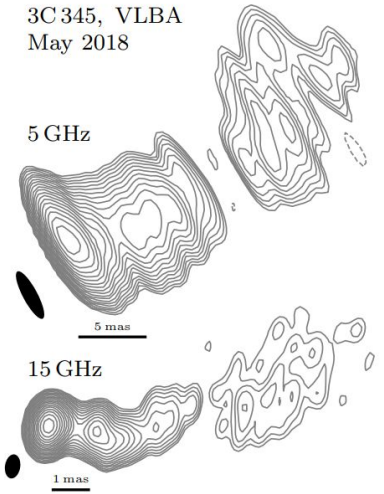

VLBA images of the total intensity radiation in the jet of 3C 345 at 5 and 15 GHz; credit: Roder et al. (2024)

What are ‘swinging’ jets?

In the literature, we encounter jets described with the terms: *curved, bent, twisted, kink, twisting, wobble, wobbling, wiggle, wiggling, swinging, oscillating…*

Curved or *bent/twisted*: a jet that presents a curvature/several curvatures in different directions (at a given time)

Kink: local protuberance of a part of the jet (at a given time)

Wiggle: generally, small-scale repetitive bends observed on the jet ridge-lines (at a given time)

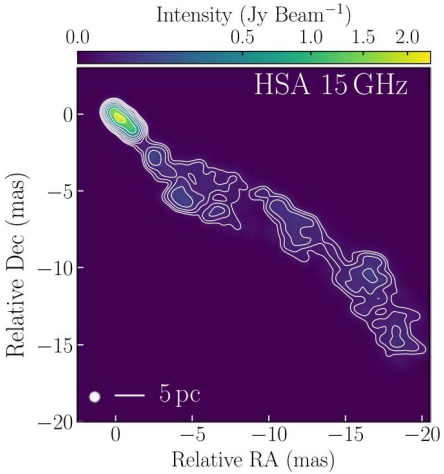

Image of the 3C 273 jet with the HSA (high sensitivity array) at 15 GHz; credit: Okino et al. (2022)

What are 'swinging' jets?

In the literature, we encounter jets described with the terms: *curved, bent, twisted, kink, twisting, wobble, wobbling, wiggle, wiggling, swinging, oscillating…*

Curved or *bent/twisted*: a jet that presents a curvature/several curvatures in different directions (at a given time)

Kink: local protuberance of a part of the jet (at a given time)

Wiggle: generally, small-scale repetitive bends observed on the jet ridge-lines (at a given time)

Twisting, wobble(ing), wiggling: generally, a jet whose morphology presents a (periodic) temporal change in its orientation

Swinging: a jet that changes orientation over time

Oscillating: a jet that changes orientation periodically over time

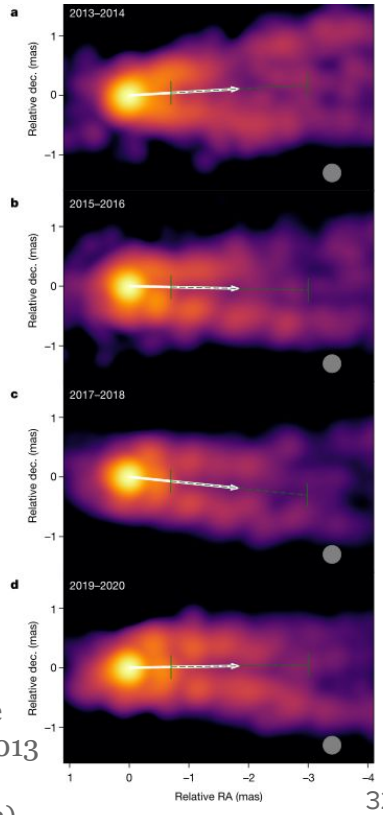

Structural evolution of the M87 jet from 2013 to 2020; credit: Cui et al. (2023)

What are 'swinging' jets?

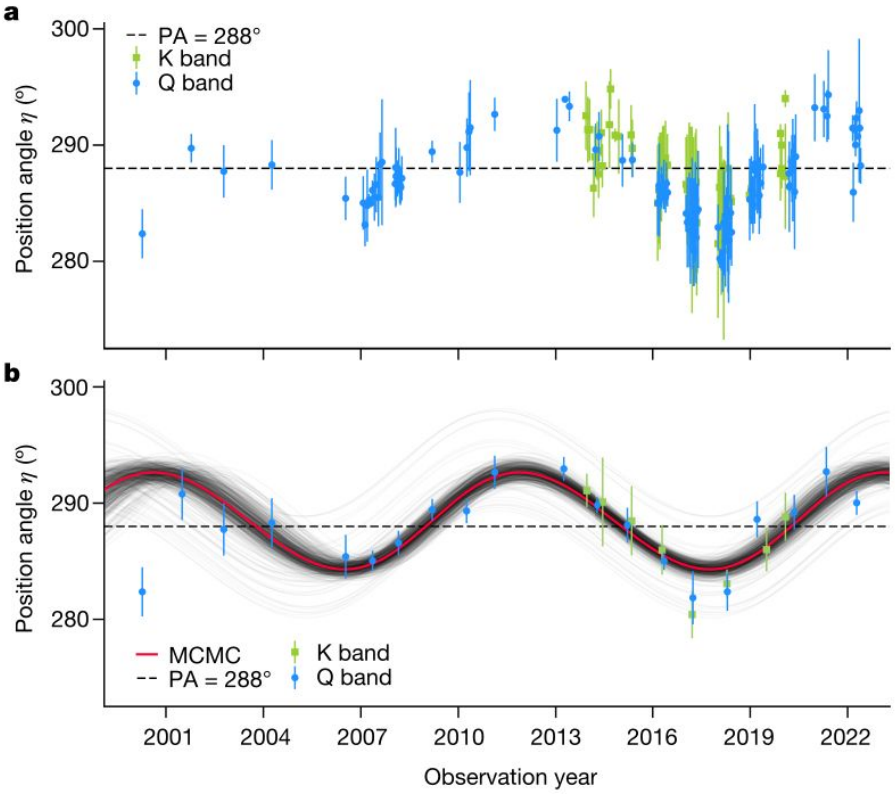

a) Evolution of the position angle (PA) of the M87 jet and b) fit of the yearly binned PA with a precession model; credit: Cui et al. (2023)

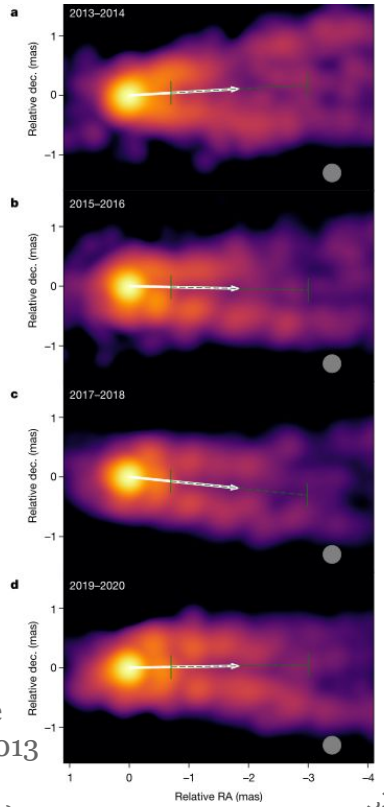

Structural evolution of the M87 jet from 2013 to 2020; credit: Cui et al. (2023)

Jet or disk precession

Lense-Thirring (LT) disk precession

b) Fit of the yearly binned M87 PA evolution with a jet precession model and
c) precessing jet model used for the fitting; credit: Cui et al. (2023)

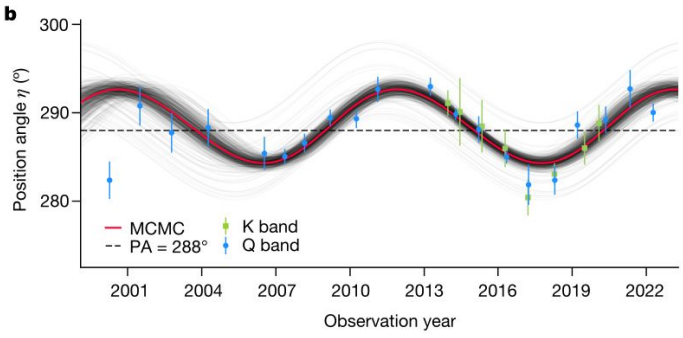

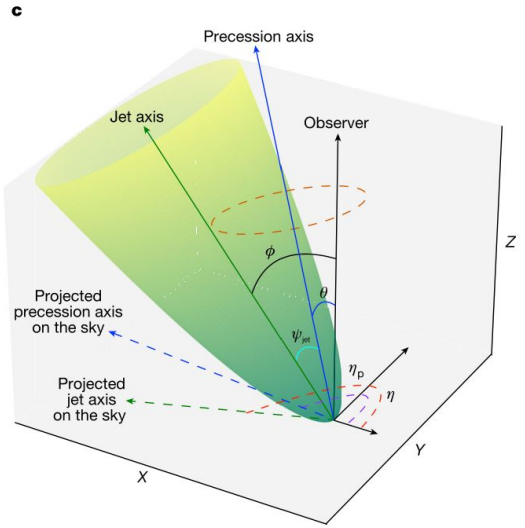

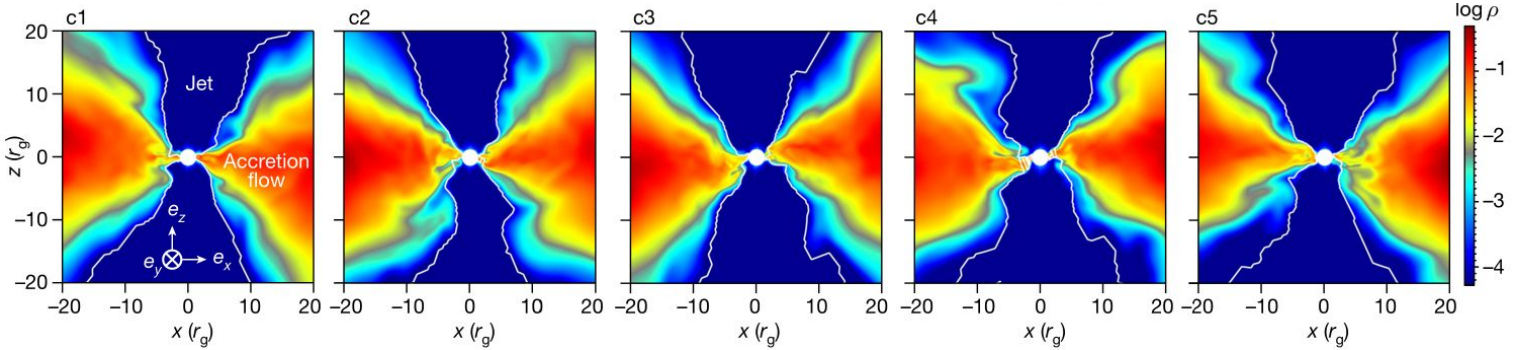

Snapshots of mass density ρ of the 3D GRMHD simulation results; credit: Cui et al. (2023)

Supermassive black hole binary system

OJ 287 is the most promising candidate SMBHB with a ~12 year periodicity in its optical light curve presenting double-peaks, associated with disturbances of the primary accretion disc caused by the plunging of the secondary BH.

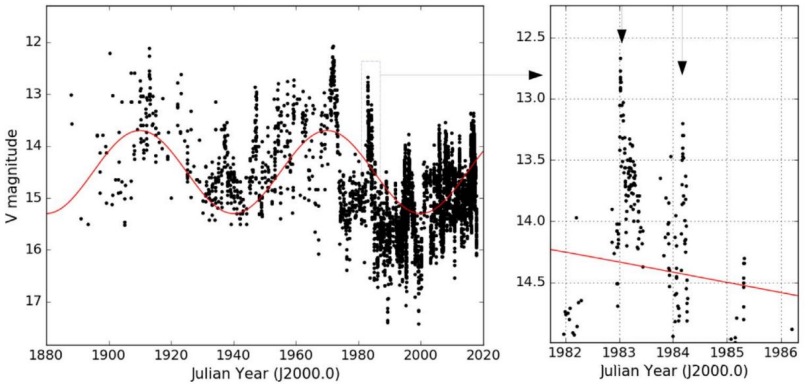

Optical light curve of OJ 287 from 1886 to 2017 with a fiducial curve for visualization of the long-term variations; and observed double-peaked structure of the high-brightness flares; credit: Dey et al. (2018)

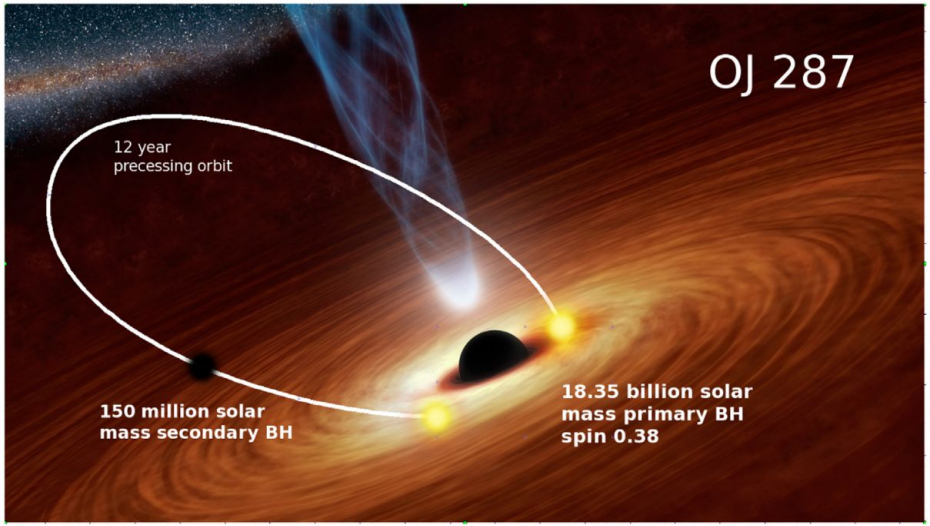

Artistic illustration of the binary black hole system in OJ 287; credit: Dey et et al. (2018)

Supermassive black hole binary system

Two year-scale timescales of OJ 287 jet oscillation favour a scenario combining orbital motion and accretion disk/orbital plane misalignment.

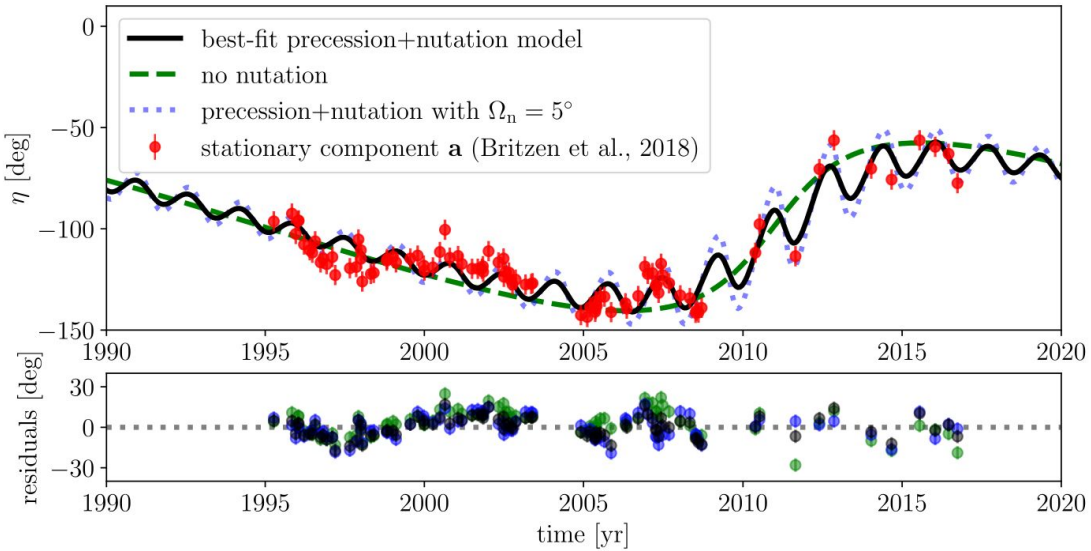

The precession-nutation model fitted to the PA evolution of the quasi-stationary component a in the jet of OJ 287: Britzen et al. (2023)

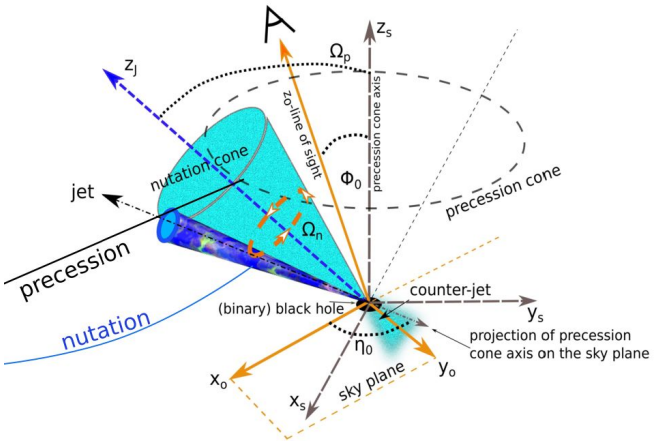

Scheme of the jet motions that in combination produce the observed variability (precession + nutation); credit: Britzen et al. (2023)

SMBHB: M 81

(A) Jet PAs observed at multi-frequencies and assembled at 8.4 GHz; .
(B) Radio light curve formed assembled at 8.4 GHz (gray: original; blue: Doppler beaming corrected);
(C) X-ray (2–10 keV) light curve (gray: original; dark: Doppler beaming corrected);
(D) Six epoch VLBI images at 8.4 GHz from 2005–2022
; credit: Jiang et al. (2023)

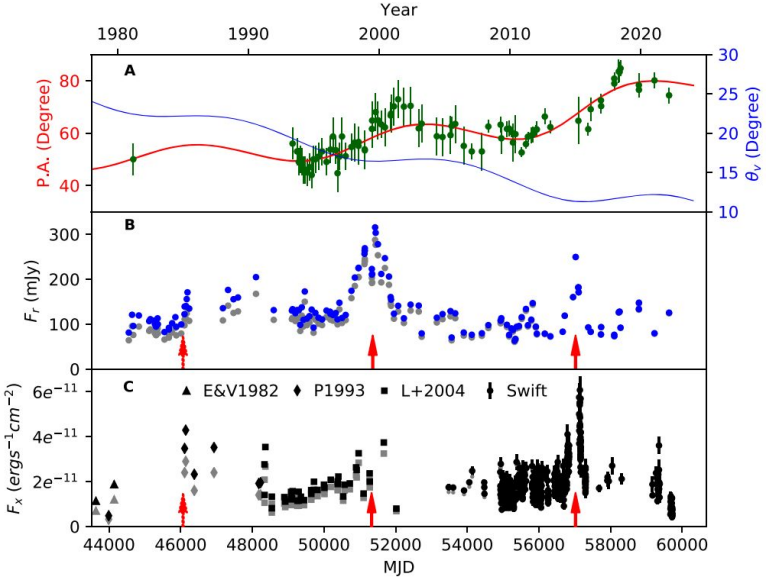

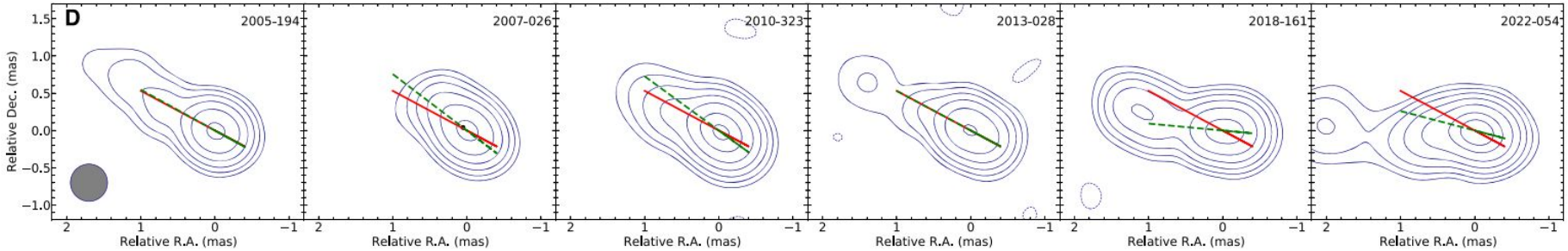

SMBHB: S5 1928+738

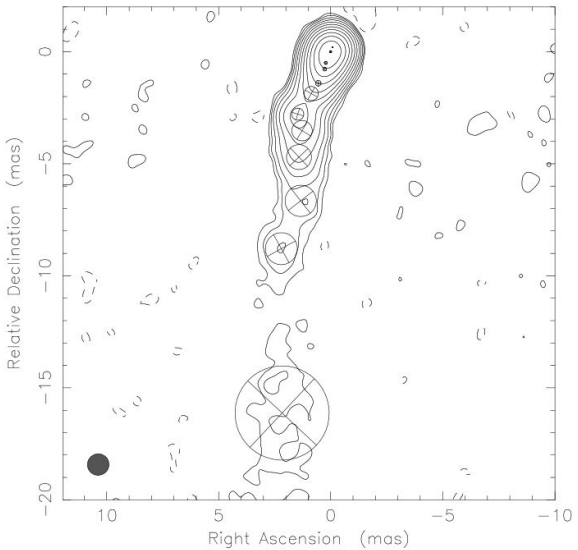

Model-fits to the 2013.06 epoch of MOJAVE observation of S5 1928+738 at 15 GHz; credit: Kun et al. (2014)

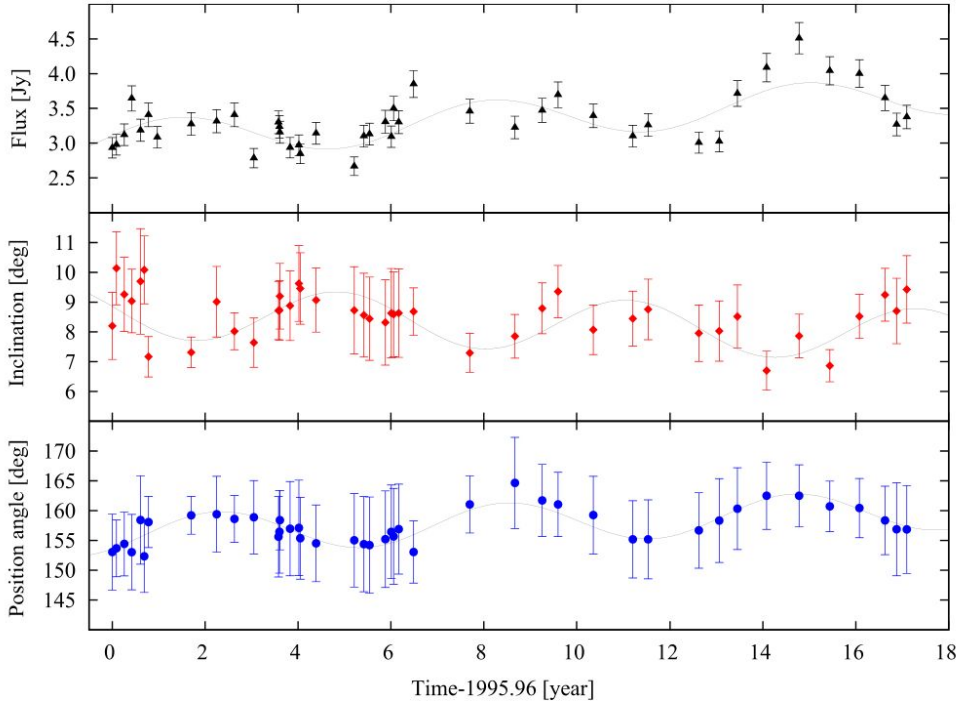

Total flux density of the jet at 15 GHz (top), inclination (middle) and position angle (bottom) of the jet geometrical axis plotted against time; credit: Kun et al. (2014)

SMBHB: S5 1928+738

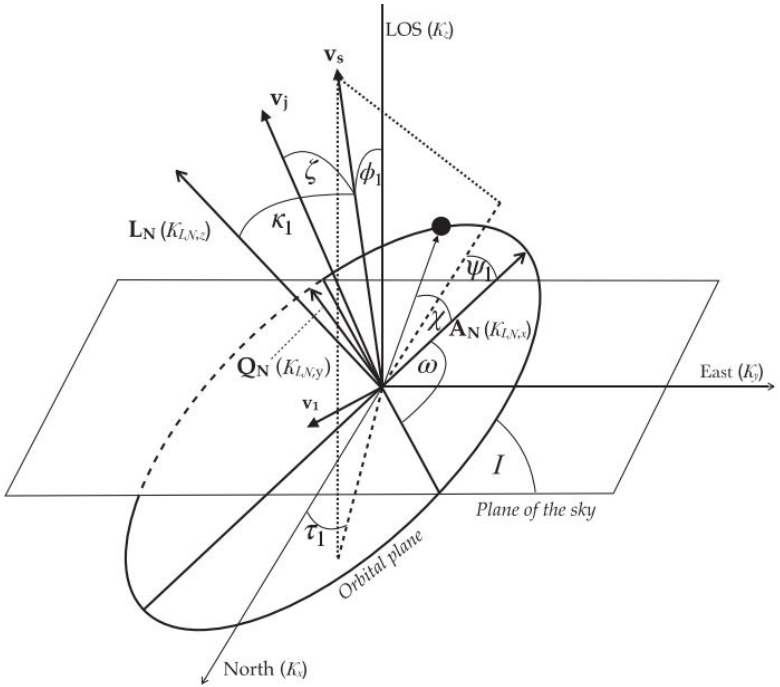

credit: Kun et al. (2023)

Figure 3. Geometric configuration of the black hole binary system centred on its barycentre. The black dot marks the position of the jet-emitting SMBH along its elliptical orbit. LOS indicates the line of sight, $\mathbf{L_N}$ is the Newtonian orbital angular momentum, $\mathbf{A_N}$ is the Laplace–Runge–Lenz vector, and $\hat{\mathbf{Q}}_\mathbf{N} = \hat{\mathbf{L}}_\mathbf{N} \times \hat{\mathbf{A}}_\mathbf{N}$. The true anomaly χ is measured from $\hat{\mathbf{A}}_\mathbf{N}$, the argument of the periapsis is ω, the orbital inclination is I, the spin angle of the dominant SMBH (which is the jet emitter) with respect to the orbital normal is κ_1, the angle between the projection of the dominant spin on to the orbital plane and the periapsis line is ψ_1 and the inclination angle of the spin with respect to the LOS is ϕ_1. The position angle of the spin projected onto the plane of the sky (τ_1) is measured from north through east. Furthermore, $\mathbf{v_1}$ is the orbital velocity vector of the dominant SMBH at the instant of the jet component launching, $\mathbf{v_s}$ is the original jet velocity vector (that is parallel to the spin), and $\mathbf{v_j}$ is the vectorial sum of these two. Finally, ζ is the instantaneous half-opening angle of the jet.

Jet or disk instabilities

Jet current-driven kink instability (CDI)

The kink instability develops in the presence of strong toroidal magnetic fields, leading to helical jet distortion.

Kruskal-Shafranov criterion: $|B_p/B_\phi| < \ell/2\pi R$

For relativistic jets (Mizuno et al. 2009): $\frac{z}{c\gamma} > 100\frac{a}{v_A}$

Ex: Interpretation for a ~13 hours quasi-periodic flux oscillation in BL Lacertae (Jorstad et al. 2022).

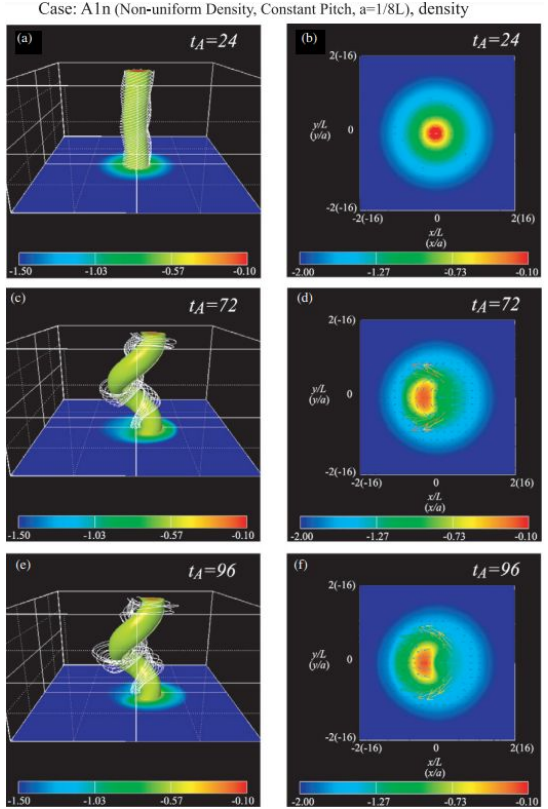

Development of the kink instability through 3D RMHD simulations; credit: Mizuno et al. (2009)

Jet or disk instabilities

Jet Kelvin-Helmholtz instability (KHI)

The KHI arises at the interface between the jet and the external medium where there is a velocity gradient. Jets may be KH unstable to *surface modes* or *body modes*.

Perturbation analysis:

$$f_1(r, \phi, z, t) = f_1(r) \exp\left[i(kz \pm n\phi - \omega t)\right]$$

The KH helical mode (n=1) has been used to explain twisted structures and swinging jets.

Ex: Interpretation of the twisted jets of 3C 449 (Hardee 1981) and of a ~10 year quasi-periodic orientation pattern in M87 (Walker et al. 2018), as well as its jet base morphology (Matveyenko & Seleznev 2015).

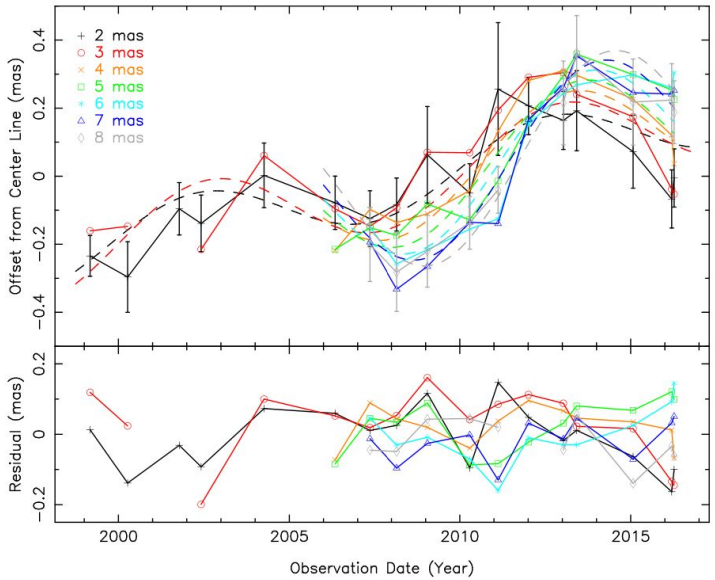

Measured offsets of the M87 jet center from a line extending from the core along position angle of −72°; credit: Walker et al. (2018)

Jet or disk instabilities

Radiation-induced disk warping

An optically thick accretion disk irradiated by a central source is unstable to becoming non-planar or warped (Pringle 1996, 1997).

In applications to AGN disks, the characteristic instability time-scale is:

$$P_{warp} \approx 2 \times 10^6 \alpha_{vis}^{-1} \frac{M}{10^8 M_\odot} \mathrm{yr}$$

Ex: Possible explanation for jet precession at the center of the galaxy NGC 1275 (Dunn et al. 2009).

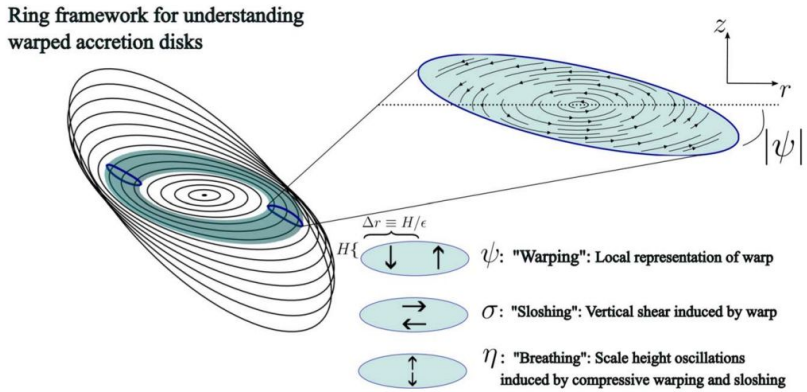

Warped disk depicted with a series of concentric annuli (black) with radially dependent orientations; credit: Kaaz et al. (2025)